A generic transport-reactive model for simulating microbially influenced mineral precipitation in porous medium

Jianchao Zhou, Andre G. van Turnhout, Michael Afanasyev, and Timo J. Heimovaara

April 13, 2015

Geo-Engineering Section, Dept. of Geoscience and Engineering, Delft University of Technology, The Netherlands

1 Introduction

The spatial and temporal distribution of precipitated minerals is one of the key factors governing various processes in the subsurface environment, including microbially influenced corrosion (MIC) (Huang, 2002), bio-cementation (van Paassen et al., 2010) and sediment diagenesis (Paraska et al., 2014). The mineral precipitation not only affects the overall reaction network (Konhauser, 1997), but is also physically interconnected with the transport properties of the subsurface environment (Pintelon et al., 2012). The presence of bacteria in the subsurface greatly influences the processes of mineral precipitation (Konhauser, 1997). We apply mathematical modeling to investigate the microbially influenced mineral precipitation process under various environmental conditions. The boundary concentrations of different solutes and the distance between the boundaries are considered to have a dominant effect on the magnitude and position and width of precipitated minerals (Gebrehiwet et al., 2014).

We study the mineral precipitation induced by MIC, a process that can be interpreted as a double diffusion mixing mineral precipitation process as shown in figure 1.1. The occurrence of biocorrosion releases metallic ion from the metal surface and creates a concentration gradient of metallic ions towards the reaction region. Released metallic ions react with existing anions, for instance carbonate, and induce a concentration gradient of anions from the distant boundary to the reaction region. The concentrations of anions at the distant boundary is continuously recharged by groundwater. Meanwhile, the concentration of metallic ions at the metal surface is maintained by the metal corrosion. The concentration gradients lead to molecular diffusion from both metal surface and distant boundary towards the reaction region, and result in mineral precipitation. Two functions of bacteria are distinguished in MIC induced mineral preciptiation: influence of biocorrosion and formation of biomass. The effects of bacteria in the double diffusion configuration are implicitly included in the iron corrosion boundary, and the biomass formation is explicitly employed in the reaction region as shown in Figure 1.1.

In terms of unlined landfills, the leakage of inorganic and organic pollutants can be interpreted as a diffusion boundary while the recharge of groundwater is treated as the other diffusion boundary. Similarly, the same double diffusion configuration can be applied to investigate the landfill leachate related mineral precipitation with the inclusion of microbial activities. The removal of heavy metals via mineral precipitation, on the one hand, helps to purify the contaminated groundwater and soil; on the other hand, the solid mass accumulation can be served as a clogging mechanism to reduce the leachate flow.

With the aid of our model, we obtain a more comprehensive insight into the relations between the development of microbially influenced mineral precipitation and the environment conditions.

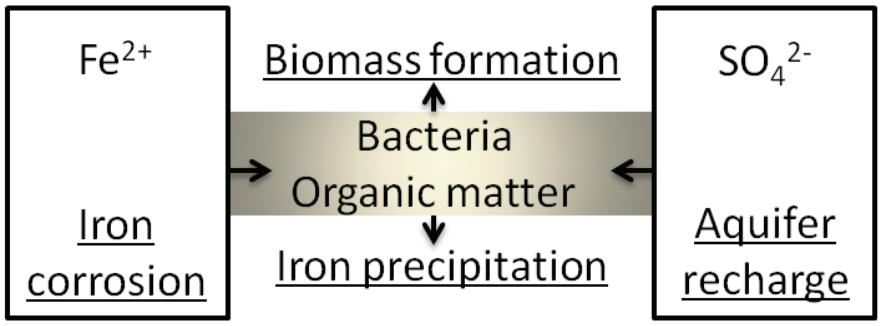

Figure 1.1: Interpretation of MIC induced mineral precipitation

2 Methods

The reactive-transport model consists of three components: MATLAB (main stream), ORCHESTRA (equilibrium reaction processor) and EXCEL (user interface) (van Turnhout et al., 2015). ORCHESTRA and MATLAB are fully coupled. This approach leads to a generic tool which we used to simulate one-dimensional flow and reactive transport in a porous environment undergoing complex biochemical reactions. Possible reactions include the kinetic phase mineral precipitation, chemical speciation reactions, kinetic biomass related reactions and gas-liquid equilibrium.

Unlike other models where physical transport medium properties are assumed to be constant, these properties in this model are interconnected through bio-chemical reactions in response to the accumulation of precipitated minerals and biomass. In this research, the phase volume changes and its effects on porosity and permeability are included. This inclusion helps to account for changes in transport properties of the porous medium due to mineral precipitation and biomass formation. The precipitated minerals and formed biomass are treated as solid mass.

For simplicity, we assume diffusive transport only, so that the physical transport equation of dissolved bio-chemical species with the inclusion of the effects of tortuosity is formulated as equation 2.1. For each aqueous component, the following mass continuity equation describes the coupling between transport process and bio-chemical process:

$$\frac{\partial}{\partial t}(\Phi \cdot C_i) = \nabla \cdot (\frac{\Phi}{F} \cdot D_i \cdot \nabla C_i) + S_i \tag{2.1}$$

$$F = \frac{1}{a\Phi^m} \tag{2.2}$$

where Φ is the porosity, C_i is the concentration of species i, F is the formation factor, S_i is the bio-chemical sink term, D_i is the dispersion tensor of species i, a is a fitted empirical constant and m is the cementation exponent. We chose to use 0.71 and 2 respectively (Oelkers, 1996).

To verify the applicability of the model, a comparison is made between our model simulation and experimental observations and model simulations implemented by Gebrehiwet et al. (2014), who used a double diffusion configuration as shown in figure 2.1. In addition, a biotic iron minerals precipitation simulation is implemented in order to illustrate the role of bacteria in mineral precipitation. The reaction networks for both cases are listed in table 2.1. In the abiotic case, a Dirichlet boundary is applied on both boundaries where the concentrations at two boundaries are fixed. In the biotic case, a Neumann boundary condition is applied on the iron corrosion boundary. The other sulfate boundary is a Dirichlet boundary. For the calcite precipitation case, the boundary concentrations are $C_{Ca^{2+}} = 0.1$ mol L^{-1} and $C_{HCO_3^-} = 0.1$ mol L^{-1} respectively. For the biotic iron minerals precipitation case, the boundary concentrations are $C_{Fe^{2+}} = 0.25$ mol L^{-1} and $C_{SO_4^{2-}} = 0.2$ mol L^{-1}. Other used parameters are listed in Appendix A.

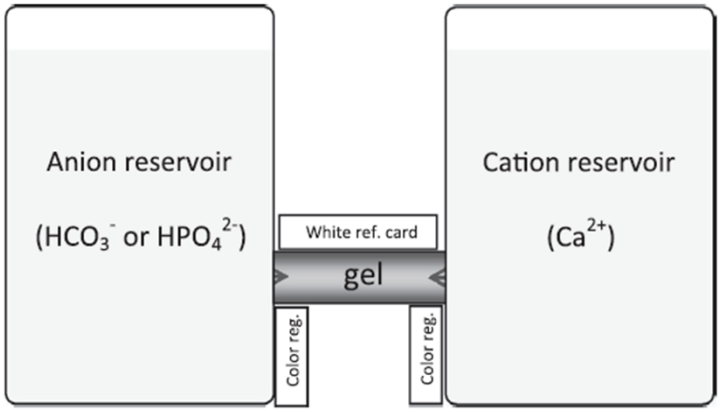

Figure 2.1: Schematic of double diffusion configuration used in the calcium precipitation experiments (Gebrehiwet et al., 2014)

Table 2.1: Reaction networks for abiotic case and biotic cases

Abiotic calcite precipitation

Kinetic reactions	Equilibrium reactions
$Ca^{2+} + HCO_3^- \rightarrow Calcite + H^+$	$H_2CO_3^* \leftrightarrow HCO_3^- + H^+$
	$HCO_3^- \leftrightarrow H^+ + CO_3^{2-}$
	$H_2O \leftrightarrow H^+ + OH^-$
	$CaHCO_3^+ \leftrightarrow H^+ + Ca^{2+} + CO_3^{2-}$
	$CaOH^+ + H^+ \leftrightarrow Ca^{2+} + H_2O$
	$CaCO_{3[aq]} \leftrightarrow CO_3^{2-} + Ca^{2+}$

Biotic iron minerals precipitation

Biomass formation	
$3.13Lac^- + 0.2NH_4^+ + 4.171SO_4^{2-} \rightarrow B_x + 8.391HCO_3^- + 4.171HS^- + 0.4H_2O + 1.29H^+$	
$B_x + 0.5H_2O \rightarrow 0.333Lac^- + 0.2NH_4^+$	
Mineral precipitations	**Equilibrium reactions**
$Fe^{2+} + HCO_3^- \rightarrow FeCO_3 + H^+$	$NH_4^+ \leftrightarrow NH_3 + H^+$
$Fe^{2+} + HS^- \rightarrow FeS + H^+$	$H_2O \leftrightarrow H^+ + OH^-$
	$H_2CO_3^* \leftrightarrow HCO_3^- + H^+$
	$HCO_3^- \leftrightarrow H^+ + CO_3^{2-}$
	$HLac \leftrightarrow Lac^- + H^+$
	$NaHCO_3 \leftrightarrow Na^+ + HCO_3^-$
	$NaCO_3^- \leftrightarrow Na^+ + CO_3^{2-}$
	$H_2S \leftrightarrow H^+ + HS^-$
	$HS^- \leftrightarrow H^+ + S^{2-}$
	$HSO_4^- \leftrightarrow H^+ + SO_4^{2-}$
	$H_2SO_4 \leftrightarrow H^+ + HSO_4^-$

Reaction reaction of abiotic clacite precipitation is took from Gebrehiwet et al. (2014).

3 Results

The model simulation results from our model are consistent with the experimental observations as well as the other modeling simulation. Similarly, the asymmetry of calcite precipitation is observed. The width of precipitated calcite zone is approximately 2 cm which is consistent with the observed 2.2 cm. As shown in figure 3.1, the simulation results from our model show

an excellent match with the experimental observations, in which precipitated calcite is visualized as white particles. The two dash red lines indicate the calcite precipitation region. The black dash line is used to identify the densest calcite precipitation position.

In the case of biotic iron minerals precipitation, the kinetics of biomass dominates the production of HS^- and HCO_3^-, which lead to iron minerals precipitation. As shown in figure 3.2, with high availability of both sulfate and lactate, biomass forms at a relatively high rate and wider range, and this is termed as first biomass growth stage. Accordingly, HS^- has a high production rate. As a consequence, the removal of HS^- via pyrrhotite precipitation as well as the regression of HS^- profile are initialized. The first growth stage lasts until lactate is depleted. Afterward, the biomass starts to decay and no more HS^- is produced, this phase is called second growth stage. Subjected to biomass growth dynamics, the precipitated pyrrhotite shows double zonations distribution while siderite precipitation does not.

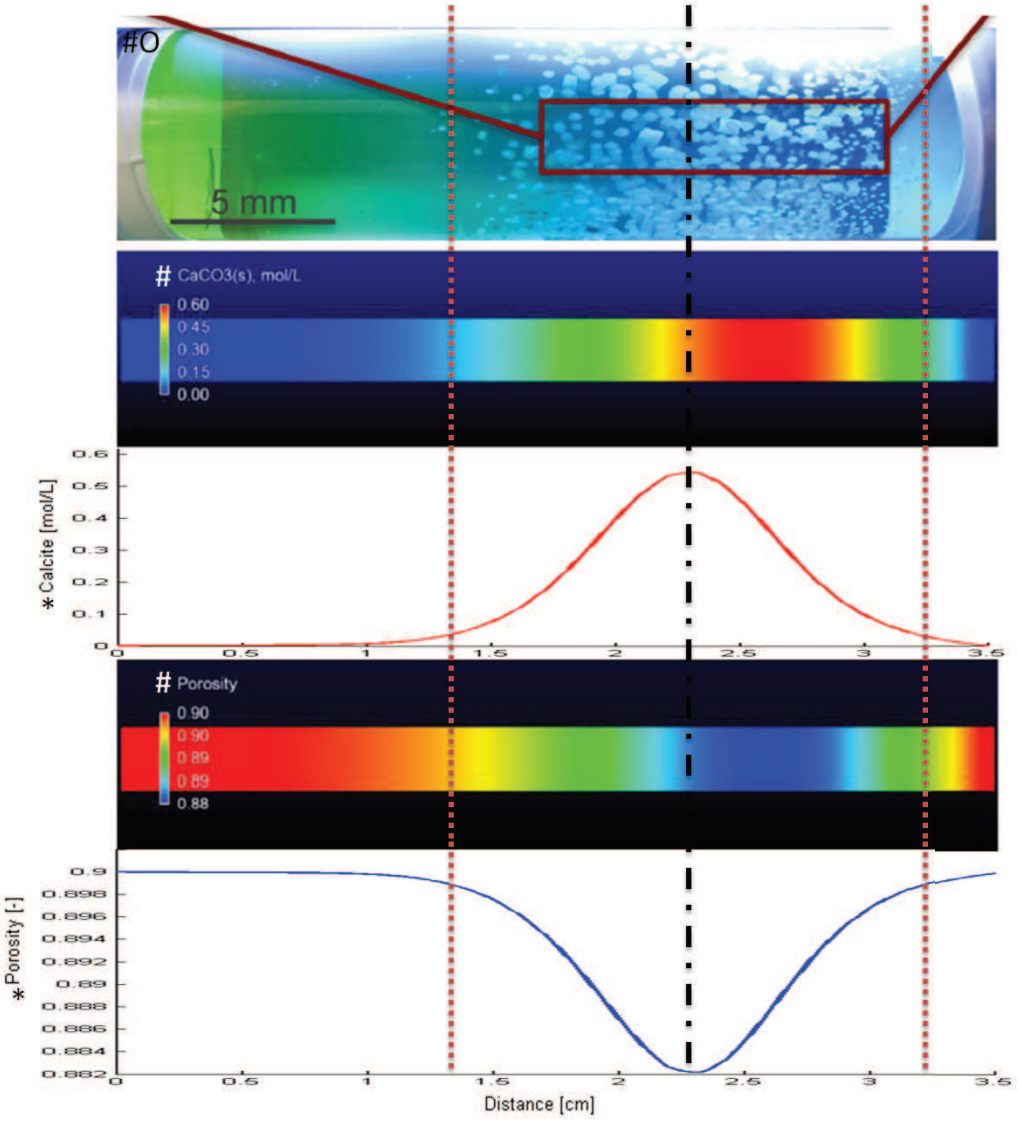

Figure 3.1: Simulation results and experimental observation for the calcite precipitation

Symbol '*' indicating simulation results from our model; symbol '#' denoting simulation results from Gebrehiwet et al. (2014); symbol '#O' denoting experimental observation from Gebrehiwet et al. (2014).

4 Discussion

The asymmetry of precipitated calcite distribution is demonstrated by both simulation results and experimental observations. It has found that the calcite precipitated close to the bicarbonate boundary. As indicated by Gebrehiwet et al. (2014), this

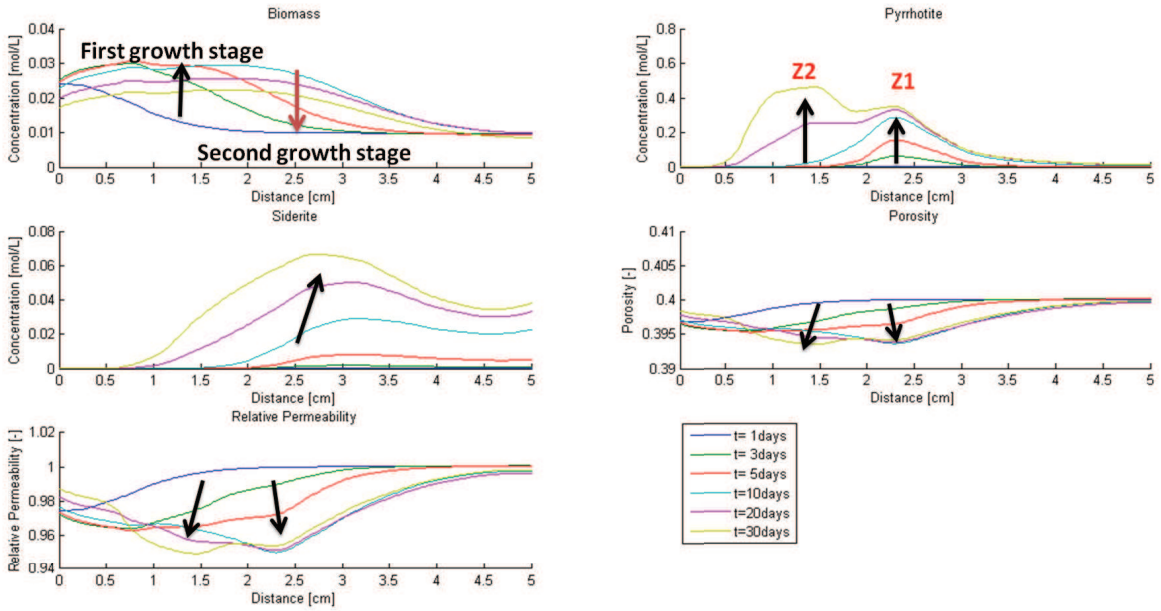

Figure 3.2: Progress of solid mass accumulation and transport properties changes in the biotic iron minerals precipitation simulation

might relate to the pH distribution. In this double diffusion configuration, the pH at the bicarbonate boundary is maintained at 9 while at the calcium side the pH is kept at 7. The precipitation of calcite from bicarbonate consumes carbonate and releases protons. Hence, calcite precipitation helps to buffer the local pH rise induced by the supply of bicarbonate near the bicarbonate boundary. Meanwhile, released protons lower the pH in vicinity to the calcium boundary. With higher pH close to the bicarbonate side, the availability of carbonate is higher accordingly. The abundance of carbonate near the bicarbonate boundary is more favorable for calcite to reach its supersaturation state. As a consequence, more calcite is precipitate near the bicarbonate boundary.

The deviation of our simulation results regarding calcite precipitation to the other simulation might because our model adopted different rate law to express the mineral precipitation. In addition, the transport process in our model is comparably more comprehensive in which effects of porosity reduction and tortuosity alteration are explicitly included.

Regarding the biotic iron minerals precipitation, the onset of microbial activities affects the spatial distribution remarkably. Those HS^- released from the fast first growth stage leads to the formation of pyrrhotite zone 1, which is signified as $Z1$ in figure 3.2. The remaining HS^- from first growth stage is continuously consumed by precipitation. The regression of HS^- combined with the progression of Fe^{2+} shifts the position of pyrrhotite precipitation backwards to the sulfate boundary and leads to the formation of pyrrhotite zone 2, $Z2$. The high solubility product of siderite significantly slows down the siderite precipitation. In other words, those HCO_3^- resealed from the first biomass growth stage are already abundant. Hence, the comparably slow siderite precipitation is unable to induce the regression of HCO_3^- profile. As a consequence, it won't have the double zonation.

5 Conclusions

The complexity of the model presented in this paper is mainly related to the comprehensive representation of the reaction network and corresponding rate relations while the transport process is kept relatively simple. In addition, the complex biofilm dynamics are ignored due to the fact that the focal point of this research is the mineral precipitation process. The results obtained, however, fit experimental data very closely and allow for a detailed investigation in precipitation dynamics and speciation. The model is also readily extensible and additional complexity can easily be added if required.

With respect to landfill research, the current setting of this model is adequate to investigate: 1) the interaction between biogeochemistry and diffusional transport where advective transport can easily be included, 2) its impact on leaching times of compounds, 3) and the dynamics of biotic heavy metal removal via mineral precipitation.

References

Gebrehiwet, T., Guo, L., Fox, D., Huang, H., Fujita, Y., Smith, R., Henriksen, J., & Redden, G. (2014). Precipitation of calcium carbonate and calcium phosphate under diffusion controlled mixing. *Applied Geochemistry*, 46, 43–56.

Huang, P. M. (2002). *Interactions Between Soil Particles and Microorganisms: Impact on the Terrestrial Ecosystem*. John Wiley & Sons.

Hunter, K., Wang, Y., & Van Cappellen, P. (1998). Kinetic modeling of microbially-driven redox chemistry of subsurface environments: coupling transport, microbial metabolism and geochemistry. *Journal of Hydrology*, 209(1-4), 53–80.

Islam, J. & Singhal, N. (2002). A one-dimensional reactive multi-component landfill leachate transport model. *Environmental Modelling & Software*, 17(6), 531–543.

Konhauser, K. (1997). Bacterial iron biomineralisation in nature. *FEMS Microbiology Reviews*, 20(3-4), 315–326.

Oelkers, E. H. (1996). Physical and chemical properties of rocks and fluids for chemical mass transport calculations. *Reviews in Mineralogy and Geochemistry*, 34(1), 131–191.

Paraska, D. W., Hipsey, M. R., & Salmon, S. U. (2014). Sediment diagenesis models: Review of approaches, challenges and opportunities. *Environmental Modelling & Software*, 61, 297–325.

Pintelon, T. R. R., Picioreanu, C., van Loosdrecht, M. C. M., & Johns, M. L. (2012). The effect of biofilm permeability on bio-clogging of porous media. *Biotechnology and bioengineering*, 109(4), 1031–42.

van Paassen, L. A., Daza, C. M., Staal, M., Sorokin, D. Y., van der Zon, W., & van Loosdrecht, M. C. (2010). Potential soil reinforcement by biological denitrification. *Ecological Engineering*, 36(2), 168–175.

van Turnhout, A. G., Kleerebezem, R., & Heimovaara, T. J. (2015). How to find the optimal mechanistic reaction network describing your data? a gray modeling toolbox developed and applied on municipal solid waste. *In review*.